Short title:

RanGAP1 and 2 are common targets of nematode and viral effectors

Title:

Two evolutionary distinct effectors from a nematode and virus target RanGAP1 and 2 via the WPP domain to promote disease

Octavina C. A Sukarta[1, a], Amalia Diaz-Granados[1, a], Erik J Slootweg[1, a], Hein Overmars[1], Casper van Schaik[1], Somnath Pokhare[2], Jan Roosien[1], Rikus Pomp[1], Abdelnaser Elashry[3,4], Geert Smant[1], Aska Goverse[1]

[1]Laboratory of Nematology, Wageningen University & Research, Wageningen, the Netherlands

[2]ICAR - National Research Centre on Pomegranate (ICAR-NRCP), Solapur- 413255, Maharashtra, India

[3]Strube Research GmbH & Co., Neue Str. 11, Schlanstedt, 38838, Germany

[4]Department of Molecular Phytomedicine, INRES, University of Bonn, Bonn, Germany

[a]These authors have equal contributions to this manuscript

[b]Corresponding author: Aska Goverse. E-mail: aska.goverse@wur.nl. Tel: +31-317485086

ABSTRACT

The Gpa2 and Rx1 intracellular immune receptors are canonical CC-NB-LRR proteins belonging to the same *R* gene cluster in potato. Despite sharing high sequence homology, they have evolved to provide defence against unrelated pathogens. Gpa2 detects Gp-RBP-1 effectors secreted by the potato cyst nematode *Globodera pallida* whereas Rx1 recognizes the viral coat protein (CP) of Potato Virus X (PVX). How Gpa2 and Rx1 perceive their matching effectors remains unknown. Using a combination of *in planta* Co-Immunoprecipitation and cellular imaging, we show that both Gp-RBP-1 and PVX-CP physically interact with RanGAP2 and RanGAP1 in the cytoplasm of plant cells. Interestingly, this was also demonstrated for the eliciting variants of Gp-RBP-1 and PVX-CP indicating a role for RanGAP1 and RanGAP2 in pathogenicity independent from Gpa2 and Rx1 recognition. Indeed, knocking down both RanGAP homologs reduce cyst nematode and PVX infection. These findings show that RanGAP1/2 act as common host targets of evolutionary distinct effectors from two plant pathogens with different lifestyles. The involvement of RanGAP1/2 to pathogen virulence is a novel role not yet reported for these key host cell components and as such, their possible role in cyst nematode parasitism and viral pathogenicity are discussed. Moreover, from these findings a model emerges for their possible role as co-factor in pathogen recognition by the potato immune receptors Gpa2/Rx1.

Keywords: virulence target, effector recognition, RanGAP2, RanGAP1, NB-LRR, Rx1, Gpa2

50 **INTRODUCTION**

51 Effective immunity hinges on the successful recognition of the invading pathogen or
52 the damage they cause. In plants, this process is mediated by a group of cell-
53 autonomous receptor proteins, most of which belong to the family of Nucleotide-
54 Binding Leucine-Rich Repeats (NB-LRR) receptors (1). Plant NB-LRR immune
55 receptors function intracellularly to detect specific pathogen-derived effector
56 molecules. In parallel, effectors evolved to manipulate host cellular processes and/or
57 suppress plant defence in favour of promoting virulence of the pathogen (2). Upon
58 effector recognition, NB-LRRs trigger a suit of defence responses that can effectively
59 suppress further infection in a process known as Effector-Triggered Immunity (ETI).
60 This often manifests in the form of localized cell death, also known as the
61 Hypersensitive Response (HR) (1).

62 Over the years, several studies have detailed how plant NB-LRRs can perceive
63 pathogens, which have advanced our understanding of the mechanistic basis of effector
64 recognition (reviewed in (1)). This includes a receptor-ligand model, which involves
65 direct interaction between the NB-LRR and its matching effector. This was first
66 documented in the rice CC-NB-LRR (CNL) Pita, for which functionality was reported
67 to be compromised when substituting a single amino acid in its Leucine-Rich Repeat
68 (LRR) domain. Such a substitution abolished interaction with the *Magnaporthe grisea*
69 effector Avr-Pita (3). It appears, however, that the direct recognition model applies only
70 to a few exceptional cases (4, 5). Instead, a majority of NB-LRRs indirectly sense
71 pathogen-induced modifications of effector targets or their mimics (4). In this manner,
72 it is believed that the plant can circumvent rapidly evolving pathogens by enabling a

73 single NB-LRR to detect multiple effectors that act on a single host target. Today, a
74 wide variety of models for pathogen detection have been described that reconcile the
75 detection of a plethora of invading pathogens with only a limited set of NB-LRR
76 immune receptors (1).
77
78 The CC-NB-LRRs Gpa2 and Rx1 from potato (*Solanum tuberosum* spp. *andigena*) are
79 highly homologous immune receptors (88% identity) that mediate distinct defense
80 responses against evolutionarily unrelated pathogens (6-8). Gpa2 confers defense
81 against the potato cyst nematode *Globodera pallida* by inducing a hypersensitive
82 response, disconnecting the nematode's feeding site from the root vasculature, resulting
83 in nematode arrest. Heterologous studies have shown, however, that Gpa2 can also
84 trigger HR in the leaves of *Nicotiana benthamiana* upon detection of the nematode-
85 secreted effector Gp-RBP-1 (9). In turn, Rx1 mediates immunity to Potato Virus X
86 (PVX), a filamentous positive-sense RNA virus that infects aerial parts of *Solanaceous*
87 plants. Upon recognition of the viral coat protein (PVX-CP), Rx1 activates a
88 symptomless defence response referred to as extreme resistance that effectively limits
89 infection to initially affected cells (7). Rx1 also has the capacity to induce a classical
90 HR, when it is overexpressed or when there is an overaccumulation of PVX-CP in
91 heterologous studies (7, 10). In contrast to the Rx1 and Gpa2 immune receptors, PVX-
92 CP and Gp-RBP-1 effectors share no sequence nor structural similarities. It is well
93 established that the recognition specificity of Rx1 and Gpa2 is confined to the C-
94 terminal end of the LRR domain (11-13). Moreover, it has been demonstrated that
95 subtle changes in amino acid residues are sufficient to evade Rx1 and Gpa2 recognition.
96 For example, the substitution of a proline by a serine in Gp-RBP-1 prevents the
97 activation of HR (Sacco et al 2009), whereas two amino acid substitutions in the PVX-

98 CP compromises Rx1 recognition (7). However, the molecular mechanisms underlying
99 effector recognition by Gpa2 and Rx1 are still unknown.
100
101 Interestingly, sequence exchange events between Rx1 and Gpa2 pinpoint to a functional
102 bifurcation of the receptor in which recognition specificity is determined by the
103 hypervariable LRR domain, whereas defence activation is confined to the CC-NB-ARC
104 moiety (12). This is consistent with findings that the N-terminal moieties of plant NB-
105 LRRs can act as scaffolds for interactions with host proteins involved in downstream
106 signalling (14). As the CC-NB-ARC is interchangeable between Gpa2 and Rx1, this
107 also suggests that both receptors are likely to share similar co-factors. Indeed, the
108 conserved CC domains of both receptors form a complex with the WPP domain of the
109 RanGTPase activating protein 2 (RanGAP2) (15, 16). RanGAP2 plays a vital role in
110 the cell by regulating mitosis and nucleocytoplasmic transport during plant
111 development (9, 17, 18). As such, RanGAP2 was shown to act as a co-factor by
112 balancing the distribution of Rx1 in the nucleus and cytoplasm as well as modulating
113 its stability (19). Although it was shown that RanGAP2 contributes to Rx1 and Gpa2-
114 mediated defence responses, the underlying mechanisms remain unclear (15, 16).
115
116 Artificial tethering of Gp-RBP-1 to RanGAP2 in a YFP-complementation experiments
117 showed that HR by Gpa2 in *N. benthamiana* is enhanced (9). This suggests that
118 RanGAP2 may contribute to Gpa2-mediated immunity by facilitating Gp-RBP-1
119 recognition. Given that RanGAP2 is also a co-factor of Rx1, we hypothesized that
120 RanGAP2 could also contribute to PVX-CP recognition through complex formation in
121 plant cells. To test whether Gp-RBP-1 and PVX-CP could associate with RanGAP2 *in*
122 *planta*, a combination of Co-Immunoprecipitation (Co-IP) and advanced cellular

123 imaging studies was performed. We were able to show that RanGAP2 can indeed form
124 protein complexes with Gp-RBP-1 and PVX-CPs *in planta* via its conserved WPP
125 domain. We could further demonstrate that these effectors also target RanGAP1, a
126 homolog shown previously to interact with Rx1 in a yeast-two-hybrid assay (19).
127 Interestingly, also non-eliciting variants of PVX-CP and Gp-RBP-1 can associate with
128 RanGAP1 and RanGAP2, suggesting a broader role for this common effector target in
129 promoting nematode and viral pathogenicity. Indeed, knocking down either or both
130 RanGAP homologs reduced infection by PVX in *N. benthamiana* and the cyst
131 nematode *Heterodera schachtii* in *Arabidopsis thaliana.* These data support a model of
132 RanGAP1/2 as a common effector target of two taxonomically distinct pathogens with
133 different modes of action, a virus and nematode. To our knowledge, this is the first
134 study demonstrating the effector targeting of RanGAP1/2 and their role in promoting
135 disease in different plant parts. Possible roles of RanGAP1/2 in cyst nematode and PVX
136 pathogenicity are discussed as well as a tripartite model for effector recognition by the
137 immune receptors Gpa2/Rx1 that emerges from our findings.

138 **RESULTS**

139 **Eliciting and non-eliciting effectors of *G. pallida* and PVX interact with full-**
140 **length RanGAP1 and RanGAP2 *in planta***

141

142 To discern whether RanGAP2 and Gp-RBP-1 can form a complex *in planta*, we
143 performed a Co-IP assay. To that end, full-length RanGAP2-GFP was co-expressed
144 transiently in leaves of *N. benthamiana* by agroinfiltration with 8×HA-tagged versions
145 of the Gpa2-activating or non-activating Gp-RBP-1 variants, namely D383-1 and
146 Rook4. In plants, RanGAP2 is homologous to RanGAP1, sharing 66.2% identity at the

147 amino acid level in *N. benthamiana*. Both protein homologs are functionally redundant
148 where they act as activators of RanGTPase as part of the nucleocytoplasmic transport
149 cycle (20, 21). We, therefore, sought to investigate whether RanGAP1 could also
150 associate with Gp-RBP-1. For Co-IP, RanGAP2-GFP or RanGAP1-GFP was captured
151 with anti-GFP (α-GFP) conjugated paramagnetic beads as bait, and the bound proteins
152 were analysed by immunoblotting (**Fig. 1A**). Our data show that there were no changes
153 in protein stability of RanGAP1-GFP, RanGAP2-GFP or the Gp-RBP-1 effectors when
154 co-expressed. Both D383-1-8×HA and Rook4-8×HA effectors specifically co-
155 immunoprecipitated with both RanGAP1-GFP and RanGAP2-GFP. Interestingly,
156 these *G. pallida* effectors co-purified more in the eluate in combination with the
157 RanGAP2 homolog compared to RanGAP1. Moreover, stronger band intensity for the
158 non-eliciting Rook4 variant compared to D383-1 was consistently observed after Co-
159 IP when RanGAP1 and RanGAP2 was used as bait. This suggests that eliciting and
160 non-eliciting Gp-RBP-1 effectors may differ in their binding affinities for RanGAP2
161 and RanGAP1. Combined, our results demonstrate that both eliciting and non-eliciting
162 Gp-RBP-1 effectors can form complexes with both RanGAP homologs *in planta*.
163
164 As RanGAP2 was initially found to be a co-factor of Rx1, we expanded our Co-IP
165 studies to explore whether RanGAP1 and/or RanGAP2 can also form a complex with
166 PVX-CP (15, 16). Full-length RanGAP1-GFP and RanGAP2-GFP were used as bait to
167 pull-down 4×HA-tagged versions of the coat proteins from the non-eliciting UK3
168 (CP106) and eliciting HB (CP105) PVX strains. In line with the interaction data for
169 Gp-RBP-1, we did not observe changes in protein stabilities of RanGAP1-GFP,
170 RanGAP2-GFP, CP105-4×HA, or CP106-4×HA upon co-expression (**Fig. 1B**). Both
171 CP106-4×HA and CP105-4×HA variants co-immunoprecipitated with RanGAP2-

172 GFP, whereas no detectable amounts were pulled down with the α-GFP beads alone.
173 Our findings, therefore, reveal that also eliciting and non-eliciting variants of PVX-CP
174 can associate with both RanGAP homologs *in planta* like Gp-RBP-1. RanGAP1 and
175 RanGAP2 are, therefore, common interactors of structurally divergent effector types
176 from taxonomically unrelated pathogens with distinct lifestyles._Notably, both viral
177 coat protein variants also consistently co-purified in lower quantities when RanGAP1-
178 GFP was used as bait compared to RanGAP2-GFP like observed for Gp-RBP-1.

179 **RanGAP1 and RanGAP2 is required for virulence by nematodes and viruses**

180

181 Given that RanGAP1 and RanGAP2 can interact with both the eliciting and non-
182 eliciting variants of PVX-CP and Gp-RBP-1, we hypothesized that plant RanGAPs
183 could fulfil a broader role beyond functioning as a co-factor in pathogen recognition.
184 For instance, the effector targeting of host proteins is known to be directly used by
185 pathogens to promote virulence (22). Thus, we investigated whether RanGAP1 and/or
186 RanGAP2 can contribute to plant susceptibility to nematode and/or viral infections. To
187 investigate the function of RanGAP1 and RanGAP2 in PVX infection, we performed
188 Tobacco Rattle Virus-based Virus-Induced Gene Silencing (TRV-VIGS) in *N.*
189 *benthamiana* using constructs described in (15, 19). Twenty-one days after inoculation
190 with TRV, leaves *N. benthamiana* plants were infiltrated with agrobacteria harbouring
191 amplicons of PVX-106 (non-eliciting) or PVX-105 (eliciting). Viral levels were
192 quantified in the infiltrated zones within 1-5 dpi by DAS-ELISA. Our data showed that
193 when RanGAP2 or RanGAP1 is silenced, significantly less viral accumulation occurs
194 compared to the TRV:GFP control irrespective of the viral strain at 3 dpi but not at 5
195 dpi (**Supplementals Fig. S5**) (**Fig. 2B**). Simultaneously silencing RanGAP1 and
196 RanGAP2 by VIGS results in greater suppression of both virus. Our TRV-VIGS data,

197 therefore, illustrate that both RanGAP2 and RanGAP1 contribute to PVX virulence in
198 *N. benthamiana*, only during the early stages of viral infection.

199 Similarly, we tested the role of RanGAP1/RanGAP2 in cyst nematode infection.
200 As TRV-VIGS of RanGAP1/2 in tomato and potato roots appeared to be inefficient
201 (**Supplemental Fig. S1)**, we took advantage of an alternative plant system to test the
202 contribution of RanGAP2 and RanGAP1 to cyst nematode parasitism. For this, the
203 *Arabidopsis thaliana* mutants *rangap1* (*rg1-1*) and *rangap2* (*rg2-2*) (23) were
204 challenged with the beet cyst nematode *Heterodera schachtii*, which has a similar mode
205 of parasitism as *G. pallida* on potato. Our data indicate that the total number of
206 nematodes infecting the roots of *rg1-1* was significantly lower as compared to the wild-
207 type control (Col-0), after 2 weeks of infection **(Fig. 2A1)**. Although this is less
208 significant in *rg2-2*, a consistently lower trend was observed between different
209 experimental repeats. In cyst nematodes, sex determination is dependent on
210 environmental conditions. Auspicious conditions favour the development of female
211 over male nematodes. Therefore, we also investigated the ratio between male and
212 female nematodes at 2 weeks post-infection. Interestingly, both *rg1-1* and *rg2-2* plants
213 harbour significantly fewer females than wild-type plants (**Fig. 2A2**). The reduction in
214 the total number of nematodes and ratio of females infecting the roots of mutant plants
215 collectively pinpoint that both RanGAP homologs contribute to the susceptibility of the
216 roots of *A. thaliana* and thus, to cyst nematode virulence. Combined with the disease
217 assay performed in *N. benthamiana*, we demonstrate that RanGAP1/2 contribute to the
218 infection of roots and shoots by cyst nematodes and PVX, respectively.

219

220

221 **Gp-RBP-1 and PVX-CP associate with the RanGAP2-WPP domain *in planta***

222

223 To gain further insight into the effector targeting of RanGAP2, we next resolved the
224 RanGAP domains involved in the association with Gp-RBP-1 and PVX-CP. Plant
225 RanGAPs are characterized by a unique, N-terminal WPP domain (so-called for a
226 conserved Tryp-Pro-Pro motif), which anchors the protein to the nuclear envelope (17).
227 To test if the WPP domain is sufficient for the interaction with *G. pallida* and PVX
228 effectors, we co-expressed GFP/CFP-tagged versions of the effectors with a RanGAP2-
229 WPP variant tagged with the red fluorescent protein mCherry and a nuclear localization
230 signal (NLS). The NLS-tagged RanGAP2-WPP was targeted to localize exclusively in
231 the nucleus. On the other hand, both Gp-RBP-1 and PVX-CP have a more or less equal
232 nucleocytoplasmic distribution (24, 25). It was anticipated that co-expressing WPP-
233 NLS-mCh would shift the subcellular localization of these effectors towards the
234 nucleus when these proteins exist in the same complex. This shift in nucleocytoplasmic
235 distribution can be quantified by determining the fluorescence intensity ratio between
236 the GFP-tagged protein in the nucleus and cytoplasm (I_N/I_C), as described previously
237 (23). Confocal imaging was performed at 2 days post infiltration (2 dpi). Free CFP,
238 which does not form a complex with the RanGAP2-WPP construct, was used as a
239 negative control. Remarkably, our imaging data show that higher fluorescent intensities
240 ratios for Rook4-GFP-4×HA, D383-1-GFP-4×HA, CFP-CP106, and CFP-CP105
241 occurred during co-expression with WPP-NLS-mCh in support of an interaction (**Fig.
242 3**). Apparently, the WPP domain of RanGAP2 is sufficient for complex formation with
243 Gp-RBP-1 and PVX-CP. The nucleocytoplasmic distribution of the CFP negative
244 control was not altered when co-expressed with the WPP-NLS-mCh construct. Overall,

245 our findings demonstrate that the association of Gp-RBP-1 and PVX-CP locates to the
246 WPP domain in RanGAP2.
247

248 **Effector targeting of RanGAP2 does not affect the RanGAP2-receptor complex**
249

250 RanGAP2 forms a heteromeric complex with Gpa2 and Rx1 *in planta*, which relies on
251 an interaction between the receptor CC domain and the RanGAP2-WPP region (15, 16,
252 26). Our data indicate that Gp-RBP-1 and PVX-CP also interact at the WPP domain. It
253 is, therefore, conceivable that effector targeting could affect the assembly of the
254 RanGAP2-receptor complex. To explore this, full-length Gpa2 N-terminally tagged
255 with 4×Myc was co-expressed with RanGAP2-GFP and either D383-1-8×HA or
256 Rook4-8×HA. The coat proteins 4×HA-CP106 and 4×HA-CP105 were also included
257 as controls as they do not activate Gpa2 but bind RanGAP2. Agroinfiltrated leaves were
258 harvested at 2 dpi, before a visible cell death response occurred and enabled sufficient
259 protein for detection by Western blot. Indeed, immunoblotting showed that co-
260 expressing these effectors did not strongly affect the protein levels of 4×Myc-Gpa2 and
261 RanGAP2-GFP at this time point (**Fig. 4A**). To study the interaction between Gpa2 and
262 RanGAP2 under influence of the co-expressed effectors, we performed a Co-IP with
263 4×Myc-Gpa2 as bait and RanGAP2-GFP as prey. RanGAP2-GFP was pulled down
264 with 4×Myc-Gpa2, but not in the absence of 4×Myc-Gpa2 as bait. Co-expressing with
265 either Gp-RBP-1 or PVX-CPs did not alter the amount of RanGAP2-GFP pulled down
266 along with 4×Myc-Gpa2 (**Fig. 4A**). Therefore, the interaction between Gpa2 and
267 RanGAP2 is not affected by the cell death eliciting variant of Gp-RBP-1 at 2 dpi.
268

269 We likewise investigated whether the complex of Rx1/RanGAP2 would be affected by
270 its interaction with PVX-CP. To test this, 4×Myc-Rx1 was co-expressed with
271 RanGAP2 and the PVX-CPs for 24 hours before the leaves were harvested. At this time
272 point, no cell death was visible, and the protein levels were sufficient for detection on
273 Western blot. Immunoblotting shows that Rx1 and RanGAP2-GFP protein levels were
274 not affected by the co-expressed effectors. Following IP using α-Myc beads, RanGAP2-
275 GFP specifically co-immunoprecipitated with 4×Myc-Rx1, but not with α-Myc beads
276 alone (**Fig. 4B**). The presence of the effectors does not interfere with the complex
277 between Rx1 and RanGAP2. These findings are in agreement with that observed for
278 Gpa2. Overall, we, therefore, conclude that the association between Gpa2 and Rx1 with
279 RanGAP2 appears unchanged by the cell death eliciting effectors at this time-point. We
280 corroborated these findings by examining the impact of effector targeting on the Rx1-
281 CC and RanGAP2 interaction alone, which does not elicit cell death. Our
282 immunoprecipitation data shows that PVX-CP and Gp-RBP-1 also do not affect
283 complex formation between Rx1-CC with the RanGAP2 (**Supplementals Fig. S2**).
284 Together, these data suggest that neither the eliciting nor non-eliciting effector variants
285 induced the dissociation of the CC for complex formation with RanGAP2.
286

287 **DISCUSSION**

288

289 The RanGAP2 protein has long been established as a co-factor of the closely-related
290 intracellular NB-LRR immune receptors Gpa2 and Rx1 (15, 16). Nevertheless, how
291 RanGAP2 functions in immunity provided by Gpa2 and Rx1 remains unclear. In this
292 study, we expand further on this function by providing evidence for the physical

293 association of RanGAP1 and RanGAP2 with the corresponding effectors of Gpa2 and
294 Rx1, namely Gp-RBP-1 and PVX-CP. Our interaction data suggest that complex
295 formation of effector variants of Gp-RBP-1 and PVX-CP with RanGAP1 and
296 RanGAP2 is independent of the recognition specificity of Rx1 and Gpa2. Moreover,
297 both RanGAP homologs contribute to infection of roots and shoots by these pathogens,
298 a role not yet reported for these key host cell components. These data combined suggest
299 that RanGAP2 and RanGAP1 are common host targets of evolutionary distinct
300 effectors from two unrelated plant pathogens with entirely different life strategies.

301 Our finding that RanGAP2 and RanGAP1 are common host targets of unrelated
302 pathogens is in line with an emerging picture that diverse pathogens utilize a small and
303 overlapping set of host proteins to benefit their fitness (27). The PVX-CP and Gp-RBP-
304 1 effectors bear no sequence or structural resemblance. Nevertheless, we show that both
305 effectors can form a heteromeric complex with RanGAP2 *in planta* (**Fig. 1A** and **1B**).
306 The convergence of multiple, unrelated effector molecules on a single host protein is
307 proposed to facilitate pathogens to shift to new hosts and/or effectively suppress
308 'defence hubs' (22). Prominent examples being the molecular chaperone EDS1 and
309 protease Rcr3 (28, 29). These common targets may fulfil a key function in a limited
310 range of cellular processes that pathogens require for survival (27). This pinpoints that
311 a fundamental cellular process regulated by RanGAP1 and RanGAP2 is targeted to
312 facilitate disease progression. This, in turn, aligns with our findings demonstrating that
313 the targeting of RanGAPs is observed for distinct pathogens in diverse plant
314 backgrounds.

315 To our knowledge, this is the first report for the role of RanGAP1 and RanGAP2 in
316 pathogenicity. Remarkably, a greater effect of the depletion of RanGAP1 was

317 consistently found during infection by cyst nematodes in *A. thaliana* as compared to
318 RanGAP2. This suggests that the RanGAP2 and RanGAP1 homologs may have a yet
319 undefined, differing role in processes that cyst nematodes exploit for their fitness.
320 Notably, Gp-RBP-1 was found to pull-down less efficiently with RanGAP1 (**Fig. 1A**).
321 Immunoblotting assays indicate that both RanGAP homologs are expressed at
322 comparable levels, minimizing the likelihood that the observed quantitative differences
323 in interaction are due to RanGAP1 being present in lower abundance. Alternatively, the
324 difference in interaction between RanGAP1 and RanGAP2 is likely caused by intrinsic
325 differences between the RanGAP2 and RanGAP1 proteins, with the *N. benthamiana*
326 homologs sharing an overall sequence identity of 66.29% (65.26% at the WPP domain
327 and 67.61% at the LRR domain). However, it remains to be determined whether the
328 differences observed in disease assays are linked to this sequence variation or binding
329 affinities of RanGAP1 and RanGAP2 with Gp-RPB-1.

330 During interphase, RanGAP is involved in the maintenance of a RanGTP/RanGDP
331 gradient required for macromolecule transport between the plant nucleus and the
332 cytoplasm (17). Interestingly, both nucleocytoplasmic trafficking, as well as mitotic
333 activity, are crucial host cell processes involved in nematode and viral pathogenicity
334 and cyst nematodes (30, 31). Cyst nematodes establish a feeding site inside the host
335 roots, which acts as a nutrient sink to support the growth and reproduction of the
336 nematode (32). The formation of such a feeding structure also called syncytium
337 involves drastic molecular and metabolic changes of the root cell, including the
338 reactivation of the cell cycle and the incorporation of neighbouring cells via progressive
339 cell wall dissolution (33). Hence, nematodes may recruit RanGAP1 and RanGAP2 to
340 modulate cellular processes involved in syncytium formation. Interestingly, previous
341 sequence analysis reveals Gp-RBP-1 to harbour high homology to Ran-binding protein,

342 RanBPM (9), further supporting the hypothesis that cyst nematodes may target
343 RanGAP1 and RanGAP2 to modulate the Ran cycle for their own benefit.

344 Like cyst nematodes plant viruses fully depend on their host cells for replication and
345 spreading disease, which could explain why they share a common host target despite a
346 different mode of action. PVX is a positive-stranded RNA virus whereby the cytoplasm
347 is their primary site of replication (34). Nonetheless, there is accumulating evidence for
348 the interplay between plant RNA viruses and the plant nucleus. In line with this, several
349 viral proteins having been described to translocate to the nucleus for functions such as
350 suppressing RNAi and/or recruit for splicing factors necessary to modulate viral mRNA
351 (35, 36). Interestingly, at least one virus is known to disrupt this gradient by targeting
352 Ran to interfere with nuclear efflux of antiviral factors (37). Thus, nucleocytoplasmic
353 trafficking may constitute an important aspect of plant-RNA virus infection. However,
354 whether targeting by PVX-CP directly impacts these RanGAP2-related functions and
355 the precise implications thereafter require more concrete molecular and biochemical
356 studies.

357 We further demonstrate that the interaction of both Gp-RBP-1 and PVX-CP locate to
358 the WPP domain of RanGAP1/2 (**Fig. 3**). The WPP domain is characteristic of a small
359 family of proteins associated to the nuclear envelope and possibly exclusive to plants
360 (reviewed in (38)). This domain mediates, together with WPP-interacting proteins
361 (WIPs) and WPP-interacting tail-anchored proteins, the localisation of the RanGAPs to
362 the outer surface of the nuclear envelope (NE) during interphase (18, 39, 40). Targeting
363 of the WPP may thus collectively disturb the cellular distribution and GAP activity of
364 RanGAP2, affecting the overall biological functions of the protein (e.g., in nuclear
365 trafficking). It would, therefore, be interesting to see how PVX and cyst nematodes

366 benefit from interacting with RanGAPs as a common virulence target during host
367 infection.

368 In addition, RanGAP2 is also a co-factor of the potato immune receptor Gpa2 and the
369 observed direct interaction between Gp-RBP-1 and RanGAP2 *in planta* is in
370 accordance with the effects of artificial tethering of Gp-RBP-1 and RanGap2 described
371 by (Sacco *el al.*, 2009). The direct interaction of RanGAP2 with Gp-RBP-1 supports
372 the idea that plant RanGAP2 may play a role in mediating the indirect recognition of
373 the effector by Gpa2 (15, 16). Moreover, the role of RanGAP2 as a cytoplasmic
374 retention factor also coincides with previous findings that Rx1 needs to be localized in
375 the cytoplasm for recognition (24). The physical association of RanGAP2 with the
376 corresponding effectors of its immune regulators reported here further reinforces this
377 model. It is worth noting that previous studies could not establish the complex
378 formation of RanGAP2 with PVX-CP by Co-IP (15). We attribute these differences to
379 variation in platforms and setups used. Most notably, earlier approaches made use of
380 C-terminally tagged PVX-CP constructs (19). Here, PVX-CP tagged at the N-terminus
381 was employed instead as the C-terminal variant has been proven to compromise viral
382 infection (25). Whether the loss of CP function is directly linked to impaired RanGAP2
383 binding also warrants further investigation.

384 Based on our data, we propose RanGAP2 could serve as a bait that facilitates direct
385 effector recognition (41). We, therefore, propose that recognition of PVX-CP/Gp-RBP-
386 1 is a two-step event according to the bait-and-switch model (41). This model involves
387 the initial 'docking' of the effectors to the bait, in this case, RanGAP2 via the WPP
388 domain. However, the landing of effectors to RanGAP2 is insufficient for recognition
389 and subsequent receptor activation, given that the non-eliciting effectors also bind.

390 Instead, docking to RanGAP2 brings the effector in closer proximity to the LRR, which
391 is then able to directly sense structural determinants on an accessible/exposed side of
392 the effector. Such a model is in accordance with the divergence of the Rx1 and Gpa2
393 LRRs to sense structurally unrelated effectors. It is also in line with our Co-IP
394 experiments showing that RanGAP2, Rx1/Gpa2, and their matching effectors may
395 possibly exist as a concurrent formation of a tripartite complex (**Fig. 5**). The function
396 we ascribe for RanGAP2 is reminiscent of that described for the extra Solanaceous
397 Domain (SD) in the Sw-5b receptor protein, which is likewise postulated to enhance
398 effector detection by the LRR when there is low amounts of the effector present (42).
399 The attributed role of RanGAP2 could be further linked to the finding that the N-
400 terminus of Gp-RBP-1 mediates the binding to RanGAP2 with variation in this region
401 having been described to contribute to the strength in inducing Gpa2-mediated HR (9)
402 Specifically, tagging Gp-RBP-1 at the N-terminus with a fluorophore prevents energy
403 transfer in FRET-FLIM assay and co-localization with a WPP-NLS construct
404 (**Supplementals Fig. S4**). This suggests that the N-terminus may be involved in
405 RanGAP2 binding. On the other hand, a proline to serine substitution at position 187 in
406 the C-terminus determines recognition specificity but is not required for the binding of
407 RanGAP (9). This polarization in regions of Gp-RBP-1 required for RanGAP2 binding
408 and recognition further reinforces the function of RanGAP2 as a molecular bait in the
409 NLR switch model as proposed (ref).

410 Alternatively, RanGAP2 could act as a effector target guarded by two NB-LRRs with
411 distinct recognition specificities. In this model, we anticipate that effector targeting of
412 RanGAP2 would perturb RanGAP1/2 and indirectly trigger recognition. However, we
413 were unable to detect any apparent changes in the stability, size, or banding pattern of
414 RanGAP1, RanGAP2 or its bound receptors in our assays. We do not rule out the

415 possibility that the effectors may impose other or more subtle modifications leading to
416 the perturbations of RanGAP1/2, which does not involve the dissociation of the
417 heteromeric complex. The role of RanGAP2 as a guardee, however, contradicts earlier
418 works detailing the lack of positively-selected residues on the RanGAP2 surface (43).
419 This is expected from a guarded host protein as it would need to co-evolve with the
420 pathogen. The future challenge therefore lies in uncovering the exact molecular basis
421 of RanGAP2-mediated activation of Rx1/Gpa2-like immune receptors by specific
422 effector variants. Our finding that Gp-RBP-1 and PVX-CP interact with RanGAP
423 homologs provides an important stepping-stone towards this goal.

424 MATERIALS AND METHODS

425 Plasmid constructs

426 To obtain Gp-RBP-1 variants D383-1 and Rook4 with N or C-terminally tagged GFP
427 or HA, the target genes were initially subcloned into the pRAP vector by NcoI/KpnI
428 digestion (44). A similar strategy was followed for cloning of CFP-tagged PVX-CPs.
429 For transient expression experiments in *N. benthamiana*, the tagged-effector constructs
430 were finally subcloned into the pBIN+ binary vector and transformed into
431 *Agrobacterium tumefaciens* strain MOG10 (6).

432

433 Heterologous expression by *A. tumefaciens* transient assay in *N. benthamiana*

434 Heterologous protein expression was carried out by *A. tumefaciens* transient assay
435 (ATTA) in plants, as described previously (24). Briefly, Agrobacteria strains carrying
436 the expression vectors were grown in Yeast Extract Broth (YEB) medium (5 g/L

437 peptone, 1 g/L yeast extract, 5 g/L beef extract, 5 g/L sucrose and 2.5 g/L NaCl and 2
438 ml 1M $MgSO_4$) overnight. Grown bacterial cells were spun down and re-suspended in
439 infiltration medium and optical densities at wavelength 600 nm (OD_{600}) were adjusted
440 to final OD_{600} values of 0.2-0.4 for all constructs in co-immunoprecipitation and
441 imaging assays unless otherwise stated. *A. tumefaciens* suspensions were then
442 infiltrated on the abaxial surface of the leaves of *N. benthamiana* plants using needleless
443 syringes. Infiltrated spots were harvested for protein extraction or examined by
444 microscopy at 2 days post infiltration (dpi).

445

446 **Transient silencing by TRV-VIGS and PVX resistance assay in *N. bethamiana***

447 Constructs used for RanGAP1, RanGAP2 and RanGAP1 + 2 TRV-VIGS silencing in
448 *N. bethamiana* are as described previously (15, 19). Agroinfiltration was performed in
449 a similar way as for the *N. benthamiana* agroinfiltrations (see above). Briefly, bacteria
450 are grown overnight in YEB medium and re-suspended in MMAi containing 200 µM
451 acetosyringone. Final OD_{600} of TRV1 and TRV:Rg1, TRV:RG1+2 or TRV:RG2 mix
452 were adjusted to 0.5 for infiltration. Infiltrated plants were grown for 21 days to allow
453 for systematic silencing before use in viral infection assays as described previously
454 ((45)). Briefly, Agrobacteria carrying amplicons for PVX105 or PVX106 were
455 infiltrated on TRV-silenced plants at OD_{600} values of 0.002. Between 1-5 dpi, 13 mm
456 leaf discs were harvested from infiltrated spots, extracted in phosphate buffer (pH = 7)
457 and finely ground using Tissuelyzer II (Qiagen) with settings of 30 seconds at 30 Hz.
458 Ground materials were incubated in a 96-well plate coated with polyclonal antibody
459 targeted against the PVX-CP (Prime Diagnostics) at 37ºC for 2 hours, before a second
460 round of incubation with a conjugate antibody carrying alkaline phosphatase. Viral

461 levels were quantified by absorbance measurements at 405 nm with the BioRad
462 microplate reader (model 680) following a reaction with the substrate *p*-Nitrophenol.
463 Statistical analyses were performed in R studio Version 1.1.456. Data from assays
464 performed in this study were checked for normality using Shapiro-Wilk Test.
465 Depending upon the outcome of the normality test, statistical level was determined
466 either by T-test or Wilcoxon-Signed Rank Test with $\alpha = 0.05$ as specified in the text.
467

468 **Virus induced gene silencing in potato or tomato**

469 Constructs used for RanGAP1 and RanGAP2 VIGS silencing in potato and tomato are
470 described previously (15, 19). Agroinfiltration was performed in a similar way as for
471 the *N. benthamiana* agroinfiltrations (see above). Briefly, bacteria are grown overnight
472 in YEB medium and re-suspended in MMA containing 200µM acetosyringone. Final
473 ODs of a TRV1 and TRV:Rg1.1, TRV:Rg1.2, TRV:RG1+2 or TRV:RG2 mix are
474 adjusted to 0.3 for infiltration in potato and to 0.4 for infiltration in tomato. Potato and
475 tomato plants are grown and maintained in silver sand under standard greenhouse
476 conditions. For nematode infection approximately 1000 eggs or 12.000 eggs of *G.*
477 *pallida* (Rookmaker) were added to the potato or tomato plants, respectively. Relative
478 gene expression was calculated with the ΔΔCt method (46)with RPN7 (47). For tomato,
479 normalization was done using the geometric mean of reference genes tubulin (48) and
480 MST1.

481

482

483

484 ***In planta* co-immunoprecipitation and detection of recombinant proteins**

485 Total protein extracts were prepared by grinding leaf material in protein extraction
486 buffer (20% (v/v) glycerol, 50 mM Tris-HCl pH 7.5, 2 mM EDTA, 300 mM NaCl, 0.6
487 mg/ml Pefabloc SC plus (Roche, Basel, Switzerland), 2% (w/v) polyclar-AT
488 polyvinylpolypyrrolidone (Serva, Heidelberg, Germany), 10 mM dithiothreitol and
489 0.1% (v/v) Tween20) on ice. For co-immunoprecipitation, protein extracts were passed
490 through a Sephadex G-25 column (GE Healthcare, Chicago, Illinois) and pre-cleared
491 by treatment with rabbit-IgG agarose (Sigma, 50 µL slurry per 60 µL protein extract).
492 The cleared protein extract was incubated with µMACS α-GFP paramagnetic (Miltenyi,
493 Bergisch Gladbach, Germany) for 1h at 4°C. Columns were washed with washing
494 buffer (20% (v/v) glycerol, 50 mM Tris-HCl pH 7.5, 2 mM EDTA, 300 mM NaCl,
495 0.10% (v/v) Nonidet 40 and 5mM dithiothreitol) five times and eluted by removing the
496 column from the uMACS collector and adding 45uL of the washing with the washing
497 solution. The input samples were mixed with 1X NuPage LDS sample buffer with 0.25
498 M dithiothreitol and incubated at 95°C for 5 minutes.

499 For Western blotting, proteins were separated by SDS-PAGE on NuPage 12% Bis-Tris
500 gels (Invitrogen) and blotted to 0.45 µm polyvinylidene difluoride membrane (Thermo
501 Scientific). Before immunodetection we blocked the membranes for 1h at room
502 temperature in 5% (w/v) powder milk in PBS with 0.1% Tween20. For
503 immunodetection rabbit α-GFP (Abcam, Cambridge, United Kingdom) with
504 horseradish peroxidase-conjugated donkey α-rabbit (Jackson ImmunoResearch, Ely,
505 United Kingdom) or horseradish peroxidase-conjugated rat α- HA (Roche) were used.
506 Peroxidase activity was visualized using SuperSignal West Femto or Dura substrate

507 (Thermo Scientific) and imaging of the luminescence with G:BOX gel documentation
508 system (Syngene, United Kingdom).

509 **Confocal laser scanning and FRET-FLIM microscopy**

510 Confocal microscopy was performed on *N. benthamiana* epidermal cells using a Zeiss
511 LSM 510 confocal microscope (Carl-Zeiss) with a 40X 1.2 numerical aperture water-
512 corrected objective. For co-localization studies the argon laser was used to excite at 488
513 nm for GFP and chlorophyll, and the HeNe laser at 543nm to excite mCherry. GFP and
514 chlorophyll emission were detected through a band-pass filter of 505 to 530nm and
515 through a 650 nm long-pass filter, respectively. mCherry emission was detected
516 through a band-pass filter of 600 to 650nm. Nuclear and cytoplasmic fluorescence
517 intensities were quantified using ImageJ (49). For FRET-FLIM analysis, the FRET
518 between GFP and mCherry was detected via Fluorescent Lifetime Imaging
519 Microscopy. The HYD SMD detector of a Leica SP5 CLSM (Leica, Wetzlar, Germany)
520 was used to measure the emission and fluorescent lifetime of GFP (495-545 nm) and
521 the red fluorescent mCh emission (570-625 nm). The excitation of the GFP
522 chromophore was measured using a white light laser (488 nm). The Time-correlated
523 single-photon counting (TCSPC) was performed using a Becker & Hickl FLIM system
524 FLIM analysis of TCSPC was performed with the B&H SPCImage software (Becker
525 & Hickl GmbH, Berlin, Germany).

526

527 **Nematode infection assays in *A. thaliana***

528 *rangap1-1* (SALK_058630) and *rangap2-2* (SALK_006398) seeds were obtained from
529 the Nottingham Arabidopsis Stock Centre (23). All *A. thaliana* genotypes used in the

530 experiments are in the Columbia 0 (Col-0) genetic background. The presence of T-
531 DNA inserts in the lines was confirmed by PCR using specific primers designed with
532 the iSect Primers tool of the SIGNAL SALK database (**Supplementals Table S1)**, in
533 combination with the universal LB primer (50). For nematode assays, seeds were
534 vapour sterilized and vernalized at $4^{O}C$ in the dark for 4 days to break seed dormancy.
535 After vernalisation the seeds were plated in pairs in 9cm petri dishes containing
536 modified KNOP medium. Plants were grown at $25^{O}C$ under a 16h/8h light-dark cycle.
537 10 day-old seedlings were inoculated with 60-70 surface-sterilized *H. schachtii*
538 infective juveniles. After 2 weeks of infection, the number of males and females present
539 in the roots of Arabidopsis plants were counted visually and the size of females and
540 syncytia were calculated with Leica M165C Binocular (Leica Microsystems, Wetzlar,
541 Germany) and the Leica Application Suite software (Leica Microsystems). To combine
542 results from 4 biological replicates, we weighted the measures of association from each
543 replicate by the inverses of their variances. The variance of such weighted average is
544 simply the inverse of the sum of the inverses of the variances which allow standard
545 methods to be used to test for the overall significance at the 5% level of the genotype
546 and the number of nematodes per plant. Such approach corresponds to methods to
547 combine studies under a fixed effects model.

548

549 **ACKNOWLEDGEMENTS**

550 The works described in this study benefits from the financial support of the COST
551 Action SUSTAIN FA1208 as well as Dutch Top Technology Institute Green Genetics
552 (5CFD051RP), Dutch Technology Hotel grant, the Dutch Technology Foundation
553 STW and Earth and Life Sciences ALW (STW-GG 14529), NWO project 828.11.002,

554 and TTI Green Genetics grant 4CC058RP which are part of the Netherlands
555 Organization for Scientific Research (NWO).We are thankful to Dr. Jan Willem Borst
556 (Laboratory of Biochemistry, Wageningen University & Research) and the
557 microspectroscopy research facility (Wageningen University & Research) for access to
558 the imaging equipments and their technical expertise. We also thank Dr. Matthieu
559 Joosten (Laboratory of Phytopathology, Wageningen University & Research) for
560 providing WPP-NLS, WPP-nls*, RanGAP1-GFP, RanGAP2-GFP and RanGAP2-
561 mCherry constructs.

562 **AUTHOR CONTRIBUTIONS**

563 Conceptualization A.G.; Methodology, O.C.A.S., and A.D.G.M; Investigation,
564 O.C.A.S., A.D.G.M, E.J.S., H.O., C.S., S.P., J.R., R.P., and A.E.; Writing – Original
565 Draft, O.C.A.S. and A.D.G.M; Writing – Review & Editing, O.C.A.S., A.D.G.M.,
566 E.J.S., A.G., and G.S; Funding Acquisition, A.G., and G.S.

567

568 **REFERENCES**

569

570 1. van Wersch S, Tian L, Hoy R, Li X. Plant NLRs: The Whistleblowers of Plant
571 Immunity. Plant Communications. 2020;1(1):100016.
572 2. Varden FA, De la Concepcion JC, Maidment JHR, Banfield MJ. Taking the
573 stage: effectors in the spotlight. Current Opinion in Plant Biology. 2017;38:25-33.
574 3. Jia Y, McAdams SA, Bryan GT, Hershey HP, Valent B. Direct interaction of
575 resistance gene and avirulence gene products confers rice blast resistance. The EMBO
576 journal. 2000;19(15):4004-14.

577 4. Dodds PN, Rathjen JP. Plant immunity: towards an integrated view of plant–
578 pathogen interactions. 2010;11:539.
579 5. Ravensdale M, Bernoux M, Ve T, Kobe B, Thrall PH, Ellis JG, et al.
580 Intramolecular Interaction Influences Binding of the Flax L5 and L6 Resistance
581 Proteins to their AvrL567 Ligands. PLOS Pathogens. 2012;8(11):e1003004.
582 6. van der Vossen EAG, van der Voort J, Kanyuka K, Bendahmane A, Sandbrink
583 H, Baulcombe DC, et al. Homologues of a single resistance-gene cluster in potato
584 confer resistance to distinct pathogens: a virus and a nematode. Plant J. 2000;23.
585 7. Bendahmane A, Köhm BA, Dedi C, Baulcombe DC. The coat protein of potato
586 virus X is a strain-specific elicitor of Rx1-mediated virus resistance in potato. The Plant
587 Journal. 1995;8(6):933-41.
588 8. Bendahmane A, Kanyuka K, Baulcombe DC. The Rx gene from potato controls
589 separate virus resistance and cell death responses. Plant Cell. 1999;11.
590 9. Sacco MA, Koropacka K, Grenier E, Jaubert MJ, Blanchard A, Goverse A, et
591 al. The cyst nematode SPRYSEC protein RBP-1 elicits Gpa2- and RanGAP2-
592 dependent plant cell death. PLoS Pathog. 2009;5.
593 10. Gilbert J, Spillane C, Kavanagh TA, Baulcombe DC. Elicitation of Rx-
594 Mediated Resistance to PVX in Potato Does Not Require New RNA Synthesis and May
595 Involve a Latent Hypersensitive Response. Molecular Plant-Microbe Interactions®.
596 1998;11(8):833-5.
597 11. Farnham G, Baulcombe DC. Artificial evolution extends the spectrum of
598 viruses that are targeted by a disease-resistance gene from potato. Proc Natl Acad Sci
599 USA. 2006;103.
600 12. Slootweg E, Koropacka K, Roosien J, Dees R, Overmars H, Lankhorst RK, et
601 al. Sequence Exchange between Homologous NB-LRR Genes Converts Virus

602 Resistance into Nematode Resistance, and Vice Versa. Plant physiology.
603 2017;175(1):498-510.
604 13. Rairdan GJ, Moffett P. Distinct Domains in the ARC Region of the Potato
605 Resistance Protein Rx Mediate LRR Binding and Inhibition of Activation. The Plant
606 Cell. 2006;18(8):2082-93.
607 14. Sun Y, Zhu Y-X, Balint-Kurti PJ, Wang G-F. Fine-Tuning Immunity: Players
608 and Regulators for Plant NLRs. Trends in Plant Science. 2020;25(7):695-713.
609 15. Tameling WIL, Baulcombe DC. Physical Association of the NB-LRR
610 Resistance Protein Rx with a Ran GTPase–Activating Protein Is Required for Extreme
611 Resistance to Potato virus X. The Plant Cell. 2007;19(5):1682-94.
612 16. Sacco MA, Mansoor S, Moffett P. A RanGAP protein physically interacts with
613 the NB-LRR protein Rx, and is required for Rx-mediated viral resistance. Plant J.
614 2007;52.
615 17. Pay A, Resch K, Frohnmeyer H, Fejes E, Nagy F, Nick P. Plant RanGAPs are
616 localized at the nuclear envelope in interphase and associated with microtubules in
617 mitotic cells. Plant J. 2002;30.
618 18. Rose A, Meier I. A domain unique to plant RanGAP is responsible for its
619 targeting to the plant nuclear rim. Proc Natl Acad Sci USA. 2001;98.
620 19. Tameling WIL, Nooijen C, Ludwig N, Boter M, Slootweg E, Goverse A, et al.
621 RanGAP2 Mediates nucleocytoplasmic partitioning of the NB-LRR immune receptor
622 Rx in the solanaceae. Thereby dictating Rx function. Plant Cell. 2010;22.
623 20. Rodrigo-Peiris T, Xu XM, Zhao Q, Wang H-J, Meier I. RanGAP is required for
624 post-meiotic mitosis in female gametophyte development in Arabidopsis thaliana.
625 Journal of Experimental Botany. 2011;62(8):2705-14.

626 21. Xu XM, Zhao Q, Rodrigo-Peiris T, Brkljacic J, He CS, Müller S, et al.
627 RanGAP1 is a continuous marker of the *Arabidopsis* cell division plane. Proceedings
628 of the National Academy of Sciences. 2008;105(47):18637-42.
629 22. Carella P, Evangelisti E, Schornack S. Sticking to it: phytopathogen effector
630 molecules may converge on evolutionarily conserved host targets in green plants.
631 Current opinion in plant biology. 2018;44:175-80.
632 23. Scholl RL, May ST, Ware DH. Seed and molecular resources for Arabidopsis.
633 Plant physiology. 2000;124(4):1477-80.
634 24. Slootweg E, Roosien J, Spiridon LN, Petrescu A-J, Tameling W, Joosten M, et
635 al. Nucleocytoplasmic distribution is required for activation of resistance by the potato
636 NB-LRR receptor Rx1 and is balanced by its functional domains. The Plant cell.
637 2010;22(12):4195-215.
638 25. Cruz SS, Chapman S, Roberts AG, Roberts IM, Prior DA, Oparka KJ. Assembly
639 and movement of a plant virus carrying a green fluorescent protein overcoat. Proc Natl
640 Acad Sci U S A. 1996;93(13):6286-90.
641 26. Hao W, Collier SM, Moffett P, Chai J. Structural basis for the interaction
642 between the potato virus X resistance protein (Rx) and its cofactor Ran GTPase-
643 activating protein 2 (RanGAP2). J Biol Chem. 2013;288(50):35868-76.
644 27. Weßling R, Epple P, Altmann S, He Y, Yang L, Henz SR, et al. Convergent
645 targeting of a common host protein-network by pathogen effectors from three kingdoms
646 of life. Cell host & microbe. 2014;16(3):364-75.
647 28. Song J, Win J, Tian M, Schornack S, Kaschani F, Ilyas M, et al. Apoplastic
648 effectors secreted by two unrelated eukaryotic plant pathogens target the tomato
649 defense protease Rcr3. Proceedings of the National Academy of Sciences.
650 2009;106(5):1654.

651 29. Bhattacharjee S, Halane MK, Kim SH, Gassmann W. Pathogen Effectors Target
652 Arabidopsis EDS1 and Alter Its Interactions with Immune Regulators Science.
653 2011;334(6061):1405-8.
654 30. Quentin M, Abad P, Favery B. Plant parasitic nematode effectors target host
655 defense and nuclear functions to establish feeding cells. Frontiers in Plant Science.
656 2013;4(53).
657 31. Liu J, Coaker G. Nuclear Trafficking During Plant Innate Immunity. Molecular
658 Plant. 2008;1(3):411-22.
659 32. Sobczak MaG, W. Cyst nematodes and syncytia. In: Genomics and molecular
660 genetics of plant-nematode interactions. Springer 2011:pp. 61-82.
661 33. de Almeida Engler J, De Vleesschauwer V, Burssens S, Celenza JL, Jr., Inze D,
662 Van Montagu M, et al. Molecular markers and cell cycle inhibitors show the importance
663 of cell cycle progression in nematode-induced galls and syncytia. Plant Cell.
664 1999;11(5):793-808.
665 34. Batten JS, Yoshinari S, Hemenway C. Potato virus X: a model system for virus
666 replication, movement and gene expression. Molecular Plant Pathology.
667 2003;4(2):125-31.
668 35. Krichevsky A, Kozlovsky SV, Gafni Y, Citovsky V. Nuclear import and export
669 of plant virus proteins and genomes. Mol Plant Pathol. 2006;7(2):131-46.
670 36. Xu M, Mazur MJ, Tao X, Kormelink R. Cellular RNA Hubs: Friends and Foes
671 of Plant Viruses. Molecular Plant-Microbe Interactions®. 2020;33(1):40-54.
672 37. Porter FW, Bochkov YA, Albee AJ, Wiese C, Palmenberg AC. A picornavirus
673 protein interacts with Ran-GTPase and disrupts nucleocytoplasmic transport.
674 Proceedings of the National Academy of Sciences of the United States of America.
675 2006;103(33):12417-22.

676 38. Meier I, Zhou X, Brkljacic J, Rose A, Zhao Q, Xu XM. Targeting proteins to
677 the plant nuclear envelope. Biochem Soc Trans. 2010;38(3):733-40.
678 39. Zhao Q, Brkljacic J, Meier I. Two distinct interacting classes of nuclear
679 envelope-associated coiled-coil proteins are required for the tissue-specific nuclear
680 envelope targeting of Arabidopsis RanGAP. Plant Cell. 2008;20(6):1639-51.
681 40. Xu XM, Meulia T, Meier I. Anchorage of plant RanGAP to the nuclear envelope
682 involves novel nuclear-pore-associated proteins. Current biology : CB.
683 2007;17(13):1157-63.
684 41. Collier SM, Moffett P. NB-LRRs work a "bait and switch" on pathogens.
685 Trends Plant Sci. 2009;14.
686 42. Li J, Huang H, Zhu M, Huang S, Zhang W, Dinesh-Kumar SP, et al. A Plant
687 Immune Receptor Adopts a Two-Step Recognition Mechanism to Enhance Viral
688 Effector Perception. Molecular Plant. 2019;12(2):248-62.
689 43. Carpentier J, Grenier E, Esquibet M, Hamel L-P, Moffett P, Manzanares-
690 Dauleux MJ, et al. Evolution and variability of Solanum RanGAP2, a cofactor in the
691 incompatible interaction between the resistance protein GPA2 and the Globodera
692 pallida effector Gp-RBP-1. BMC Evolutionary Biology. 2013;13(1):1-14.
693 44. Schouten A, Roosien J, de Boer JM, Wilmink A, Rosso M-N, Bosch D, et al.
694 Improving scFv antibody expression levels in the plant cytosol 1. FEBS Letters.
695 1997;415(2):235-41.
696 45. Slootweg EJ, Spiridon LN, Martin EC, Tameling WIL, Townsend PD, Pomp R,
697 et al. Distinct Roles of Non-Overlapping Surface Regions of the Coiled-Coil Domain
698 in the Potato Immune Receptor Rx1. Plant physiology. 2018;178(3):1310-31.
699 46. Schmittgen TD, Livak KJ. Analyzing real-time PCR data by the comparative
700 C(T) method. Nat Protoc. 2008;3(6):1101-8.

701 47. Castro-Quezada P, Aarrouf J, Claverie M, Favery B, Mugniéry D, Lefebvre V,
702 et al. Identification of reference genes for normalizing RNA expression in potato roots
703 infected with cyst nematodes. Plant molecular biology reporter. 2013;31(4):936-45.
704 48. Aimé S, Alabouvette C, Steinberg C, Olivain C. The Endophytic Strain
705 Fusarium oxysporum Fo47: A Good Candidate for Priming the Defense Responses in
706 Tomato Roots. Molecular Plant-Microbe Interactions®. 2013;26(8):918-26.
707 49. Schindelin J, Arganda-Carreras I, Frise E, Kaynig V, Longair M, Pietzsch T, et
708 al. Fiji: an open-source platform for biological-image analysis. Nat Methods.
709 2012;9(7):676-82.
710 50. Alonso JM, Stepanova AN, Leisse TJ, Kim CJ, Chen H, Shinn P, et al. Genome-
711 Wide Insertional Mutagenesis of <em>Arabidopsis thaliana</em&gt. Science.
712 2003;301(5633):653.

713

714

715

716

717

718

719

720

721

722 **FIGURE LEGENDS**

723 **Fig. 1 Gp-RBP-1 of *G. pallida* and CP of PVX associate with RanGAP1 and**
724 **RanGAP2 *in planta*.** Co-immunoprecipitation of full-length RanGAP1-GFP or
725 RanGAP2-GFP as bait and HA-tagged Gp-RBP-1 (**A**) or PVX-CP (**B**) effector proteins.
726 *A. tumefaciens* harbouring constructs for the pull-downs were co-expressed in *N.*
727 *benthamiana* leaves and harvested at 2 dpi. "+" indicates the presence of a construct in
728 the infiltration combination. The soluble extract was used for Co-IP studies using α-
729 GFP conjugated beads to precipitate the bait. The immunoblots (IB) with α-GFP and
730 α-HA antibodies of the input material are shown in the top half of the image and the
731 results of Co-IP in the two bottom panels of the figure. Coomassie brilliant blue (CBB)
732 stained blots serve as a loading control for the input material. Data shown are
733 representative of three independent repeats.

734

735 **Fig. 2. RanGAP1/2 contributes to pathogenicity of cyst nematodes in *A. thaliana***
736 **and PVX in *N. benthamiana*. A).** The total (**A1**) and average number of female and
737 male (**A2**) nematodes per plant in *A. thaliana* roots after 2 weeks of infection. Boxes
738 indicate the 75th and 25th percentile, and whiskers show the 95th and 5th percentile.
739 Data is combined from 4 individual experiments with means weighted by the inverse
740 of the variance of each replicate for (A1) **p-value <0.001, *' p-value=0.054 with n
741 *rg1-1* = 58, n *rg2-2* = 54 and n Col-0 = 65, for (A2) *p-value = 0.027 with n *rg1-1* =
742 58, n *rg2-2* = 54 and n Col-0 = 65. **B).** PVX virulence assay on TRV-VIGS *N.*
743 *benthamiana* plants silenced for RanGAP2, RanGAP1 or combinations thereof in *N.*
744 *benthamiana*. Silenced plants were infiltrated at 21 days post TRV-VIGS treatment
745 with Agrobacteria for expression of the amplicon of either PVX105 or PVX106.
746 Infiltrated leaf samples were harvested at 3 dpi for viral quantification by DAS-ELISA.

747 Statistically significant difference was compared to TRV:GFP samples using the
748 Wilcoxon-Signed Rank test ($\alpha = 0.05$) with n = 24 for all samples represented. *p-value
749 <0.05 and **p-value <0.001.
750
751 **Fig. 3. The WPP domain of RanGAP2 is sufficient for the interaction with Gp-**
752 **RBP-1 (A) and PVX-CP (B).** Representative confocal images of nuclei (N) and
753 surrounding cytoplasm (C) of cells expressing mCherry-tagged RanGAP2-WPP and
754 GFP-tagged Gp-RBP-1 (Rook4 or D383-1) (**A1**) or CFP-tagged PVX-CP constructs
755 (PVX-CP 106 or 105) (**B1**). The CFP/GFP and mCherry channels are shown side by
756 side for each combination. Quantification of the fluorescence intensity ratios (I_N/I_C
757 ratio) is represented in the accompanying boxplots (**A2** and **B2**). Boxes indicate the
758 interquartile range with whiskers indicating the maximum and minimum values.
759 Statistical significance difference was calculated using the Wilcoxon-Signed Ranked
760 test with $\alpha = 0.05$ with *p-value <0.05 and **p-value <0.001. For both PVX-CP and
761 Gp-RBP-1, data shown is the combination of at least two independent repeats.
762
763 **Fig. 4. Effector targeting of RanGAP2 does not hamper its association with Gpa2**
764 **and Rx1.** Shown in the figure are immunoblots from Co-IP experiments where 4×Myc-
765 tagged Gpa2 or Rx1 constructs were used as bait and RanGAP2-GFP as prey. HA-
766 tagged versions of CP106, CP105, or the Gp-RBP-1 D383-1 and Rook4 were
767 additionally co-expressed. The top three immunoblot (IB) panels represent the input
768 material. Coomassie brilliant blue (CBB) stained blots on which RuBisCO is visible
769 are used as a control for equal loading for the input material. The lower three panels
770 show the protein pulled down in the α-Myc immunoprecipitation. **A).** Co-
771 immunoprecipitation to test if the interaction between full-length Gpa2 and RanGAP2

772 is affected by the eliciting and non-eliciting PVX-CPs or by the Gp-RBPs D383-1 or
773 Rook4. The samples were harvested at 48 hours post agroinfiltration before cell death
774 would occur in the combination of Gpa2 and D383-1. **B).** Co-immunoprecipitation to
775 test if the interaction between full-length Rx1 and RanGAP2 is affected by the same
776 sets of effectors as in (**A**). The proteins were co-expressed for 24 hours and harvested
777 before cell death would occur in the combination of Rx1 and CP106. Data shown is
778 representative of three independent repeats. "+" indicates the presence of a construct in
779 the infiltration combination. Coomassie brilliant blue (CBB) stained blots serve as a
780 loading control for the input material.
781

782 **Fig. 5. Working model for the dual role of RanGAP1/2 in pathogen virulence (A)**
783 **and recognition events by Gpa2/Rx1 (B).** In the latter case, a model for only
784 RanGAP2 is shown, for which a clearer role in resistance of Gpa2 and Rx1 has been
785 established. **A).** In the absence of a matching NB-LRR receptor, Gp-RBP-1 and PVX-
786 CP effectors target both RanGAP1 and RanGAP2 via the WPP to promote viral disease
787 and nematode feeding cell formation in a yet undisclosed manner (**red circle**). **B**).
788 When Rx1/Gpa2 is present, the receptors tether to RanGAP1 and RanGAP2 at the
789 nuclear envelope via its WPP domain (**B1**). During invasion, both eliciting and non-
790 eliciting forms of Gp-RBP-1 and PVX-CP (orange pentagon labelled 'E') initially dock
791 to RanGAP2, bringing the effector in close proximity to the immune receptor (**B2**) to
792 facilitate recognition. Successful recognition leads to downstream events towards
793 defence.

794

795

FIGURES

Figure 1.

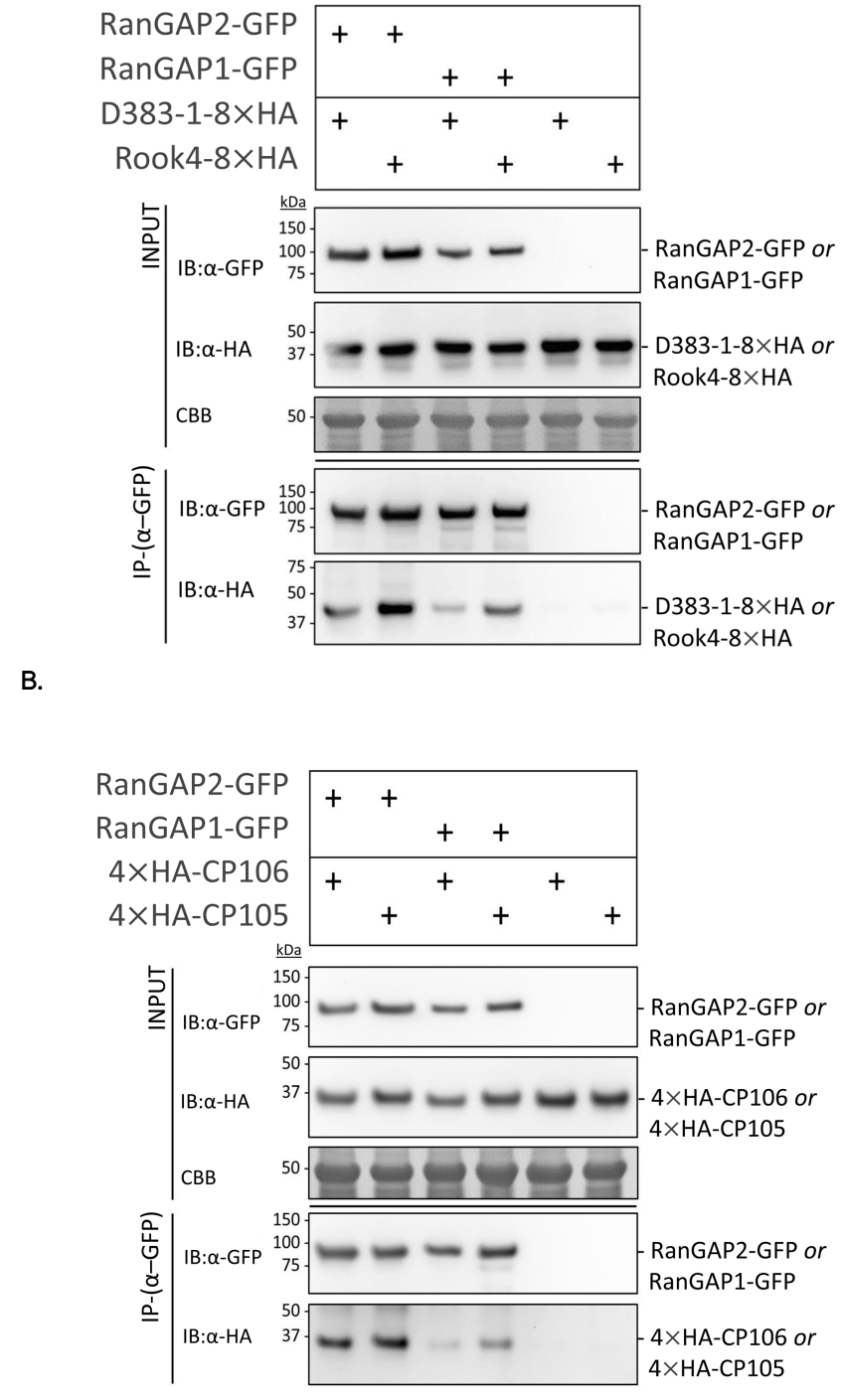

Figure 2.

A1.

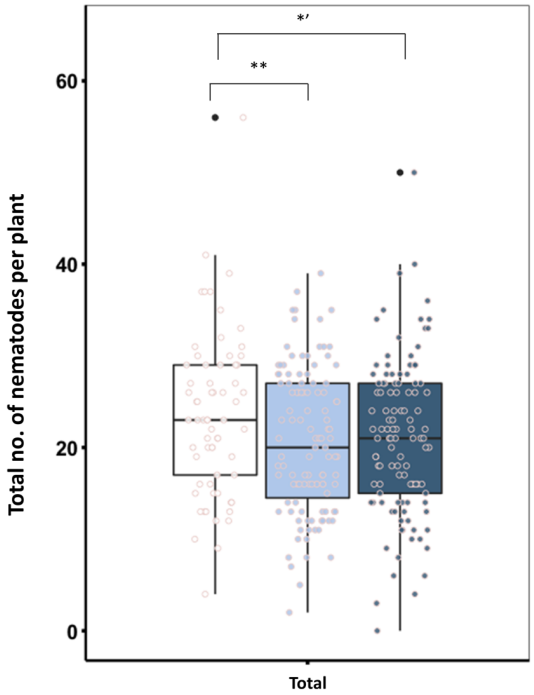

A2.

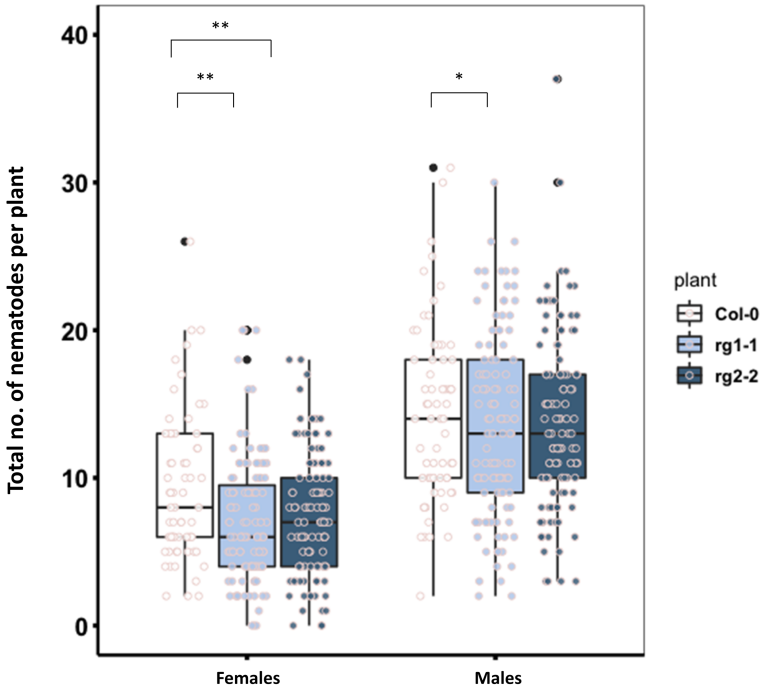

B.

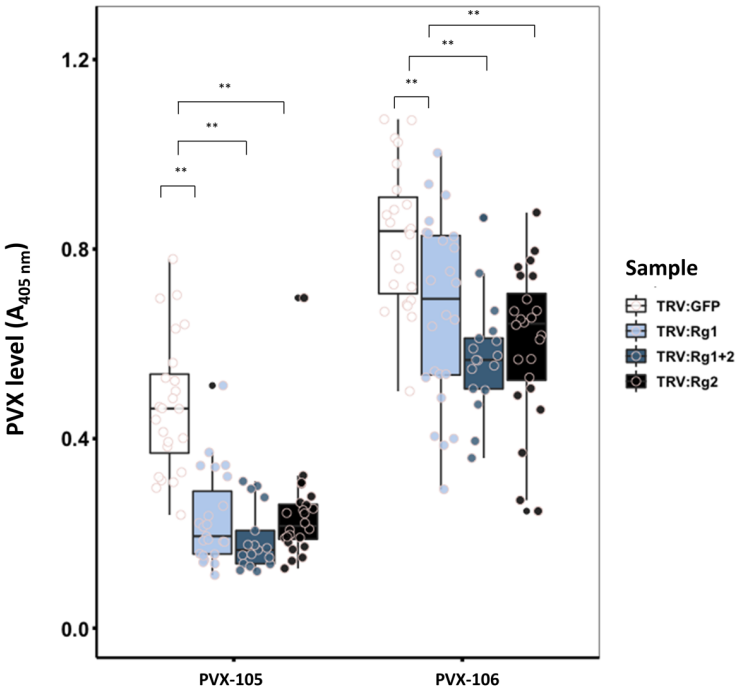

Figure 3.

A1.

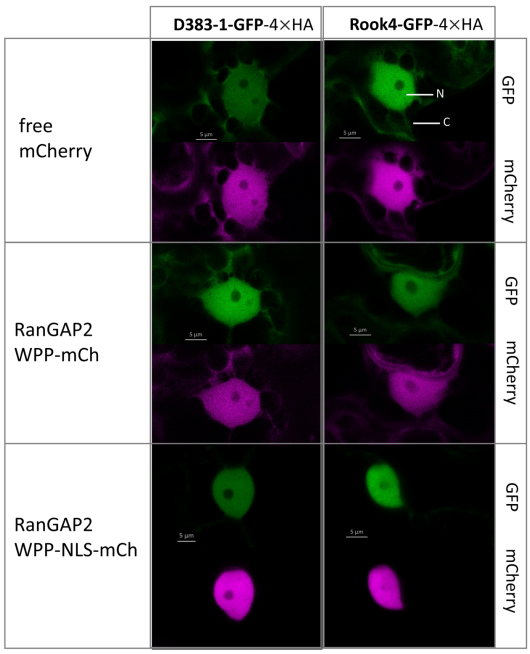

A2.

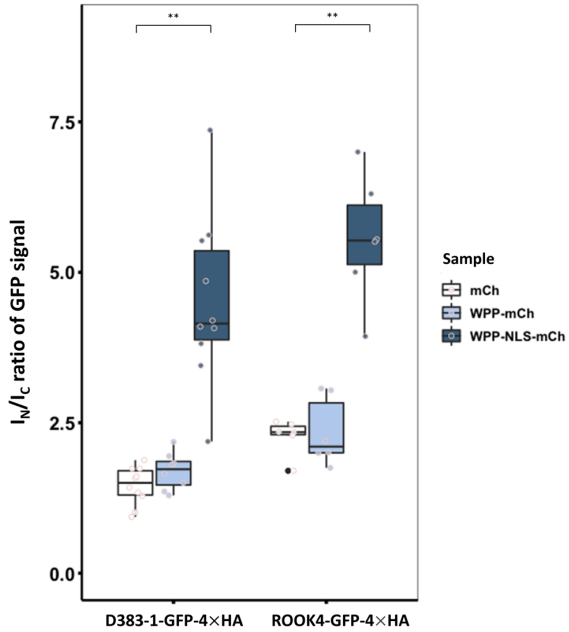

B1.

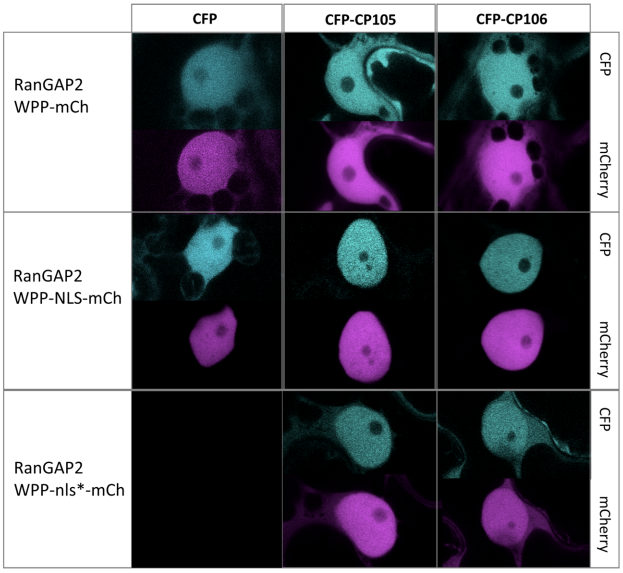

B2.

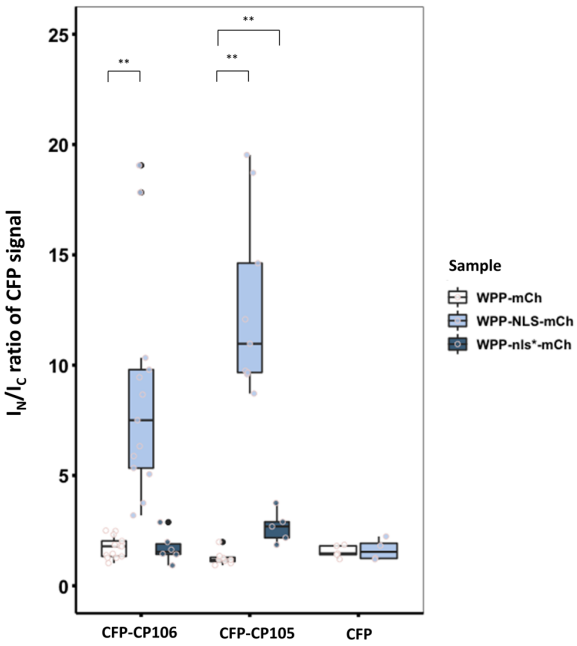

847 **Figure 4.**

848

A

849

850

851

852

853

854

855

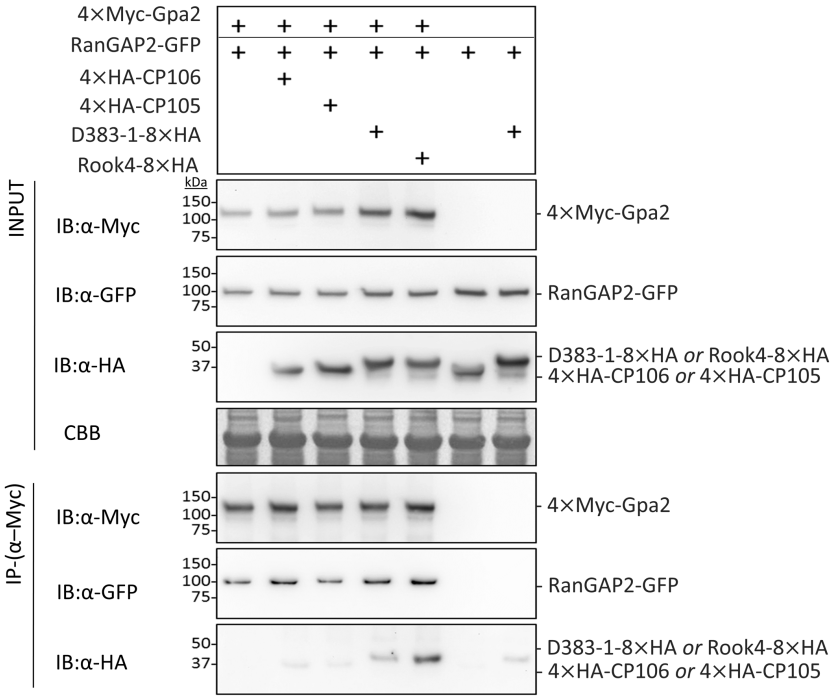

856

B.

857

858

859

860

861

862

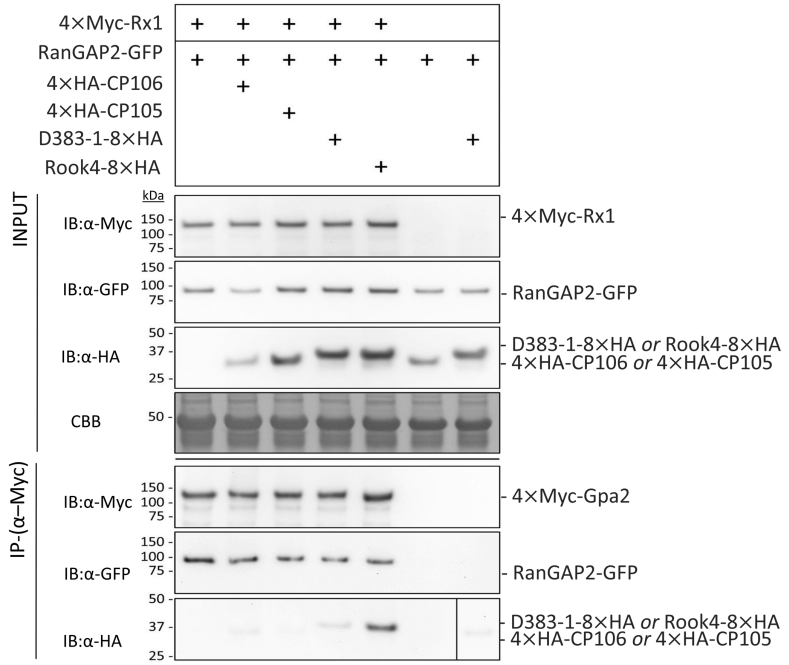

863

Figure 5.

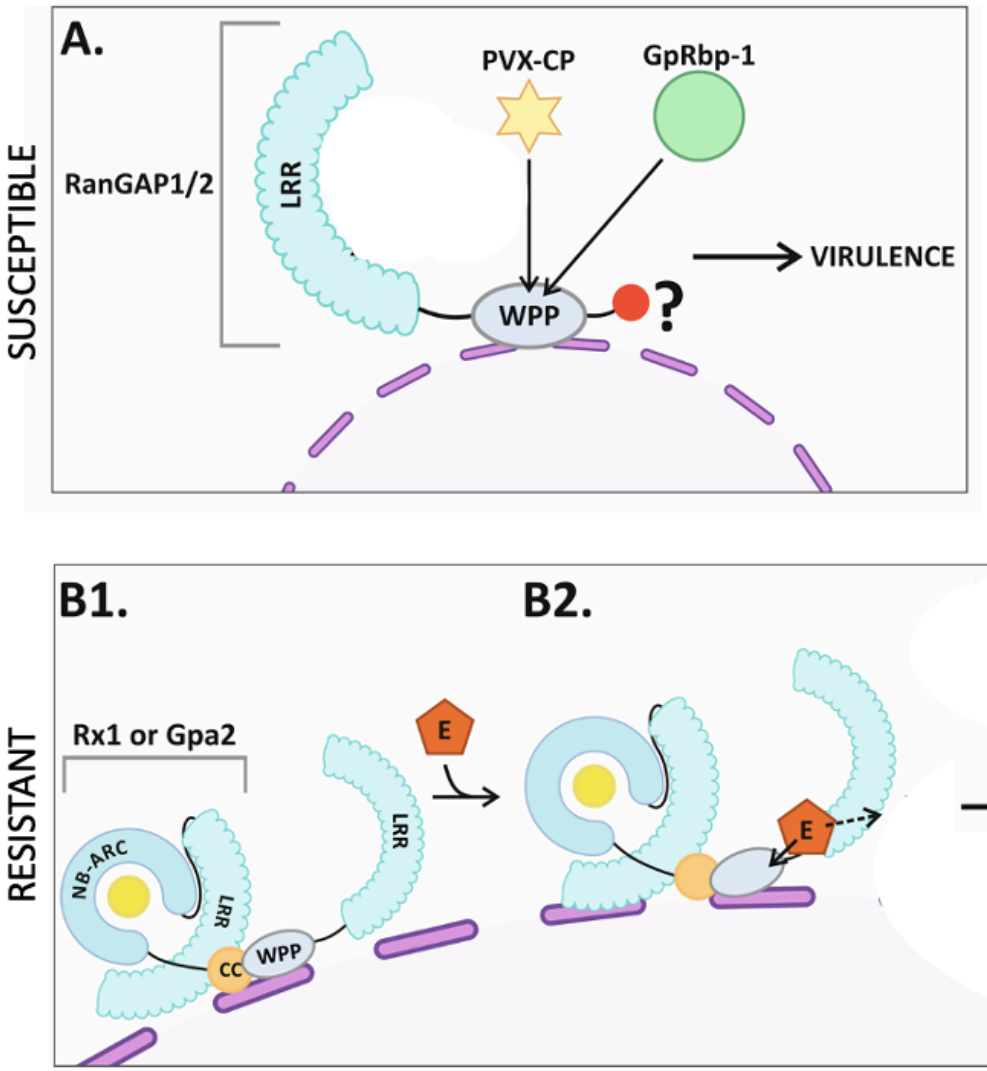
A.
SUSCEPTIBLE
RanGAP1/2
LRR
PVX-CP
GpRbp-1
WPP
?
VIRULENCE
B1.
B2.
RESISTANT
Rx1 or Gpa2
NB-ARC
LRR
CC
WPP
E
LRR
E
DEFENCE

881 **SUPPORTING INFORMATION CAPTIONS**

882 **Supplemental Table S1.** Identity percentage of RanGAP2 and RanGAP1 sequences
883 from potato, tomato and *N. benthamiana*

884 **Supplemental Fig. S1 Inefficient silencing of RanGAP1/2 in roots of tomato**
885 (***Solanum lycopersicum***) **and potato** (***Solanum tuberosum***). Tobacco rattle virus
886 (TRV) carrying guide DNA fragments targeting RanGAP1 (RG1_a and RG1_b),
887 RanGAP2(RG2), both homologues (RG1+2) or green fluorescent protein as negative
888 control was inoculated to the leaves of 10-day old tomato seedlings to induce transient
889 virus-induced silencing of RanGAP1/2. **A)** RanGAP1 or **B)** RanGAP2 expression was
890 measured by quantitative RT-PCR in TRV-infected plants and compared to the
891 expression on TRV-GFP-infected plants. Values are normalized to the geometric mean
892 of reference genes tubulin (Aimé et al., 2013) and MST1. Individual samples are
893 composed of ~10 plants/construct and RT-PCR measurements are performed in
894 triplicate. TRV-mediated silencing was quantified 3 weeks after inoculation in the
895 leaves of inoculated plants. Silencing was efficient for RanGAP1 using construct
896 RG1_a **C)** 3 weeks after TRV infection plants were inoculated with ~12000 eggs of *G.*
897 *pallida* (Rookmaker) and were grown for 2 months to allow completion of the
898 nematode life cycle. After 2 months of nematode inoculation, cysts were extracted and
899 counted from the complete root systems of plants with efficient RanGAP1 silencing.
900 **D)** a similar set-up was used for TRV-mediated transient silencing in potato, with
901 inoculum being ~1000 eggs. Cysts present in the roots of VIGS-potato were extracted
902 and quantified and no difference was found between mean amount of cysts present in
903 potatoes inoculated with RG1, RG2, RG1/2 and GFP-silencing TRV.

904 **Supplemental Fig. S2 Supporting Figure 3.** Expression of **A)** *RanGAP2* and **B)**
905 *RanGAP2* in the roots of *H. schachtii*-inoculated *Arabidopsis*, after 2, 7, 10 and 14 days
906 of inoculation. Expression compared to mock-inoculated plants was determined by
907 quantitative RT-PCR. The relative expression of RanGAP1 and RanGAP2 was
908 normalised to the geometric mean of reference genes Ubiquitin 5 (Anwer et al., 2018)
909 and ubiquitin carboxyl-terminal hydrolase 22 (Hofmann & Grundler, 2007). **C)** Size of
910 female nematodes and syncytia established in the roots of *rg1-1* and *rg2-2*, with Col-0
911 as wild-type control. Sizes are shown in mm^2. Data from 4 biological repeats is
912 combined, with means weighted by the inverse of the variance of each biological repeat.
913 Stars indicate a significant difference as established by a linear fit, * p-value= 0.015
914 with $n_{rg1\text{-}1}$ = 109, $n_{rg2\text{-}2}$ = 80 and $n_{Col\text{-}0}$= 129

915 **Supplemental Fig. S3 The binding of RanGAP2 to the CC domain of Rx1 is not**
916 **disrupted in the presence of the effectors studied.** Co-immunoprecipitation
917 investigating whether the interaction between the CC domain of Rx1 and RanGAP2 is
918 affected by the coat proteins of non-eliciting and eliciting PVX-CP strains or by the
919 Gp-RBPs D383-1 or Rook4. The samples were harvested at 48 hours post
920 agroinfiltration. As a control for aspecific binding, 4×Myc-GFP was used as bait. "+"
921 indicates the presence of a construct in the co-expressed combination.

922

923 **Supplemental Fig. S4. Tagging Gp-RBP-1 with a fluorescence protein at the N-**
924 **terminus impairs its interaction with RanGAP2 (WPP domain). A).** Confocal
925 imaging of RanGAP2-WPP-NLS constructs co-expressed with Rook4 or D383-1
926 tagged with GFP at the N or C termini. Representative images of nuclei in infiltrated
927 *N. benthamiana* epidermal cells for combinations involving N-terminally tagged Gp-
928 RBP-1s are given in **A1**. Key: N = nucleus; C = cytoplasm. Quantification of cellular

929 distribution by I_N/I_C measurements is summarized in boxplot of **A2** with boxes
930 representing the interquartile range. Data shown is the combination of two experimental
931 repeats. **B).** Boxplot indicating lifetime (picoseconds) from a FRET-FLIM experiment
932 whereby full length RanGAP2-WPP-mCh is co-expressed with the same set of effectors
933 as described in **A2**. Data shown is pooled from three experimental repeats.
934
935 **Supplemental Fig. S5.** PVX virulence assay on TRV-VIGS *N. benthamiana* plants
936 silenced for RanGAP2 in *N. benthamiana*. Silenced plants were infiltrated at 21 days
937 post TRV-VIGS treatment with Agrobacteria for expression of the amplicon of either
938 PVX105 or PVX106. Infiltrated leaf samples were harvested at 5 dpi for viral
939 quantification by DAS-ELISA. Statistically significant difference was compared to
940 TRV:GFP samples using the Wilcoxon-Signed Rank test ($\alpha = 0.05$) with $n = 8$ for all
941 samples represented.
942
943 **Supplemental Table S2.** List of primers used in the study for the genotyping of *A.*
944 *thaliana* RanGAP mutants.
945
946
947
948
949